

# “Metaphilic” Cell-Penetrating Polypeptide-Vancomycin Conjugate Efficiently Eradicates Intracellular Bacteria via a Dual Mechanism

Yunjiang Jiang, Ming Han, Yang Bo, Yujun Feng, Wenming Li, Jason Ren Wu, Ziyuan Song, Zihao Zhao, Zhengzhong Tan, Yingying Chen, Tianrui Xue, Zihuan Fu, Shanny Hsuan Kuo, Gee W. Lau, Erik Luijten,\* and Jianjun Cheng\*



Cite This: *ACS Cent. Sci.* 2020, 6, 2267–2276



Read Online

ACCESS |



Metrics & More

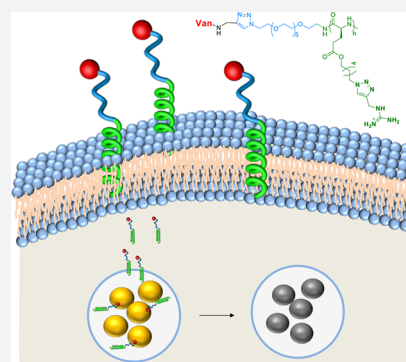


Article Recommendations



Supporting Information

**ABSTRACT:** Infections by intracellular pathogens are difficult to treat because of the poor accessibility of antibiotics to the pathogens encased by host cell membranes. As such, a strategy that can improve the membrane permeability of antibiotics would significantly increase their efficiency against the intracellular pathogens. Here, we report the design of an adaptive, metaphilic cell-penetrating polypeptide (CPP)–antibiotic conjugate (VPP-G) that can effectively eradicate the intracellular bacteria both *in vitro* and *in vivo*. VPP-G was synthesized by attaching vancomycin to a highly membrane-penetrative guanidinium-functionalized metaphilic CPP. VPP-G effectively kills not only extracellular but also far more challenging intracellular pathogens, such as *S. aureus*, methicillin-resistant *S. aureus*, and vancomycin-resistant *Enterococci*. VPP-G enters the host cell via a unique metaphilic membrane penetration mechanism and kills intracellular bacteria through disruption of both cell wall biosynthesis and membrane integrity. This dual antimicrobial mechanism of VPP-G prevents bacteria from developing drug resistance and could also potentially kill dormant intracellular bacteria. VPP-G effectively eradicates MRSA *in vivo*, significantly outperforming vancomycin, which represents one of the most effective intracellular antibacterial agents reported so far. This strategy can be easily adapted to develop other conjugates against different intracellular pathogens by attaching different antibiotics to these highly membrane-penetrative metaphilic CPPs.



## INTRODUCTION

*S. aureus* colonizes one-third of the world population and is one of the leading causes of bacterial infections globally.<sup>1</sup> In addition to the commonly known skin infections, bloodstream *S. aureus* also causes various life-threatening diseases, including endocarditis, osteomyelitis, necrotizing pneumonia, sepsis, and other deep-seated abscesses in virtually every organ.<sup>2</sup> In 2017, approximately 120,000 *S. aureus* bloodstream infections and 20,000 associated deaths were reported in the United States alone.<sup>3</sup> The high rate of treatment failure is usually associated with the rapid expansion of drug-resistant strains, such as methicillin-resistant *S. aureus* (MRSA) and vancomycin-resistant *S. aureus* (VRSA), and their capability to form biofilms. Even worse, though traditionally regarded as an extracellular pathogen, increasing evidence has shown that *S. aureus* can invade and survive inside of host cells.<sup>4–7</sup> Similar to other intracellular pathogens, including *M. tuberculosis*, *S. enterica*, and *C. trachomatis*, *S. aureus* has evolved several mechanisms to interfere with phagosome maturation and maintain its viability in the intracellular environment. *S. aureus* can either replicate in phagosomes by blocking the acidification process, inhibiting the activation of the NADPH oxidase, and preventing the fusion of phagosome with lysosome, or escape into the cytosol in an  $\alpha$ -toxin-dependent manner.<sup>8–11</sup> The

invasion into host cells protects *S. aureus* from both antibiotics and host immune systems.<sup>12,13</sup> Sporadic redissemination of intracellular bacteria contributes to treatment failure and recurring infection.

Despite the availability of many highly effective antibiotics against extracellular *S. aureus*, the options for treating intracellular *S. aureus* are limited, due to the poor membrane permeability of many hydrophilic antibiotics.<sup>14,15</sup> Vancomycin is the top-line antibiotic used for MRSA infection treatment, but has poor membrane permeability because of its high hydrophilicity and is therefore ineffective against intracellular MRSA.<sup>14,16</sup> Increasing the hydrophobicity of antibiotics improves their activity against intracellular MRSA, as in the case of rifampin, tetracyclines, and fluoroquinolones. However, their intracellular antibacterial activity is still significantly dampened compared to their extracellular antibacterial activity.<sup>17,18</sup> Moreover, intracellular *S. aureus* is rapidly

Received: July 6, 2020

Published: December 3, 2020



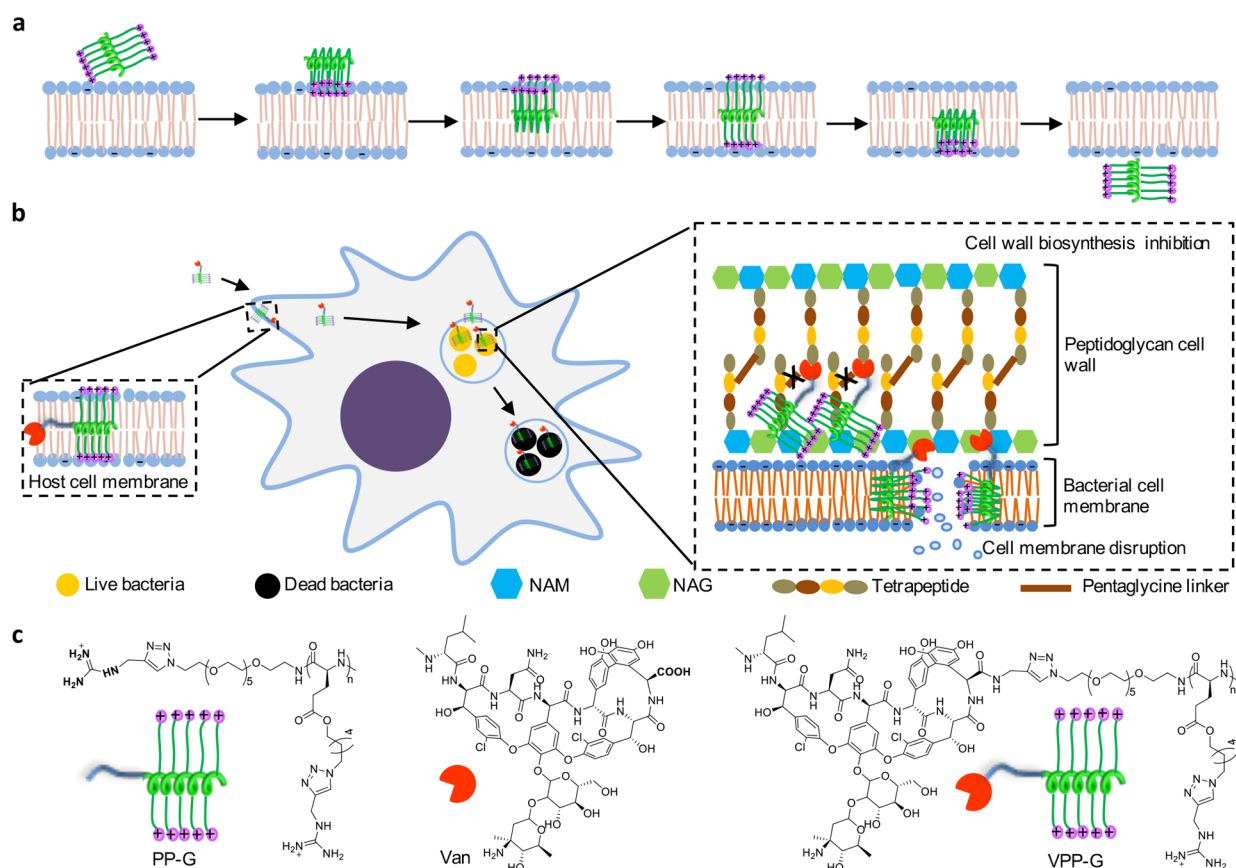


**Figure 1.** Metaphilic CPP–vancomycin conjugate VPP-G for eradication of intracellular pathogens. (a) Illustration of the membrane penetration process of metaphilic CPPs. (b) Schematic representation of the membrane penetration of VPP-G and its interaction with intracellular bacteria via a dual antimicrobial mechanism: cell wall biosynthesis inhibition and membrane disruption. NAM: N-acetylmuramic acid; NAG: N-acetylglucosamine; Tetrapeptide: (L-Ala)-(D-Gln)-(L-Lys)-(D-Ala). (c) Structure of PP-G, vancomycin (Van), and VPP-G.

developing resistance to these conventional antibiotics, which further narrows down the available choices of drugs for its treatment. Many antibiotic delivery systems based on lipid, polymer, or silica nanoparticles have also been developed for intracellular *S. aureus* clearance.<sup>19–23</sup> Although some of these systems have demonstrated intracellular delivery of a wide range of antibiotics and good bacteria reduction, they suffer from instability in biological fluids, difficulties in drug loading and formulation control, poor endosomal escape capability, and insufficient *in vivo* efficacy.<sup>24,25</sup> Moreover, many conventional antibiotics, even if they can be delivered intracellularly, are largely ineffective against dormant intracellular bacteria that may become infectious at any given time. Alternative approaches are needed to eradicate these intracellular bacteria.

In line with the recent progress in peptide–drug conjugates for targeted delivery,<sup>26</sup> there has been growing interest in developing cell-penetrating polypeptide (CPP)–antibiotic conjugates for eradicating intracellular pathogens.<sup>24,27–29</sup> Current designs of CPP–antibiotic conjugates are largely based on HIV-TAT peptide or its analogues,<sup>24,27–30</sup> which typically are arginine-rich peptides with short side chains. These CPPs enter cells through complex mechanisms. While some studies showed that CPPs enter cell through direct membrane penetration, others reported that CPPs induce membrane multilamellarity and subsequently enter cells via membrane fusion or endocytosis.<sup>31–33</sup> In both cases, the cooperation of multiple polypeptides and a relatively high threshold CPP concentration are required for membrane

penetration.<sup>31,32</sup> Such mechanisms usually result in low membrane permeability and drug delivery efficacy. It is therefore not surprising that the CPP–antibiotic conjugates based on these CPPs show only moderate intracellular antimicrobial activities.

Increasing the membrane permeability and intracellular accumulation of antibiotics are crucial to the development of potent agents against intracellular pathogens. We hypothesized that CPP–antibiotic conjugates based on peptides with antimicrobial activity and high membrane permeability may lead to complete killing of intracellular bacteria. Following this direction, we have developed a class of metaphilic CPPs with simple architecture but very high membrane permeability (up to 100-fold higher than conventional CPPs such as TAT and oligo-arginines)<sup>34–37</sup> and an unprecedented membrane-penetration mechanism (Figure 1a).<sup>38</sup> The metaphilic CPPs are a class of bottlebrush-like, radially amphiphilic polypeptides with a rigid helical core to which are attached long hydrophobic side chains (11–18  $\sigma$ -bonds) terminated with cationic groups. The helical structure is stabilized by the long hydrophobic side chains which balance the side-chain electrostatic repulsion with hydrophobic effects.<sup>34,39</sup> Both helical structure and long side-chains were demonstrated to play an important role in membrane penetration.<sup>34,37,38</sup> Like organisms that adapt to different colored environments via metachrosis, this molecular architecture adapts to different membrane environments (aqueous phase, surface charge, amphiphilic interface, hydrophobic lipid core) by being “metaphilic” rather than statically

amphiphilic, enabling its unusual interactions with membranes that are not found in other CPPs with short side chains. In the aqueous phase, metaphilic CPPs have a homogeneously distributed surface charge. When approaching a cell membrane, the CPPs start to land onto the cell membrane via the peptide/membrane surface charge interaction and gradually reorient orthogonally so that more of the charged side chains are able to reach the membrane. After this landing process, the CPPs redistribute their surface charge to one side and submerge into the lipid interior orthogonally with the other exposed hydrophobic side. Because the length of their side chains is comparable to the thickness of a lipid bilayer, and the driving force provided by the more negatively charged inner leaflet, the side chains can then further this charge redistribution through tunneling of the charge groups from the outer leaflet to the inner leaflet, realizing complete membrane penetration. This membrane-spanning process facilitates the generation of negative Gaussian curvature needed for membrane penetration.<sup>38</sup> Moreover, such a mechanism does not require the cooperation of multiple CPPs or a high threshold concentration, and may allow the direct penetration of individual polypeptides. Thanks to this unique membrane interaction mechanism, metaphilic peptides display remarkable membrane activity, including superior membrane permeability and antibacterial activities.<sup>40–42</sup>

In the case when vancomycin is conjugated to these metaphilic CPPs, we envisioned potentially unprecedented activities of the resulting conjugates against intracellular bacteria because of their superior membrane permeability and unique penetrating mechanism. Here, we report the conjugation of vancomycin to a highly membrane-active guanidinium-functionalized metaphilic polypeptide PP-G to yield conjugate vancomycin-PP-G (VPP-G, Figure 1b and c). VPP-G is remarkably potent and kills >99.9% of intracellular *S. aureus* at 9  $\mu\text{M}$ , showing dramatically improved (more than 80-fold) intracellular antimicrobial activity compared to free vancomycin, which is essentially one of the most active CPP-antibiotic conjugates reported so far. Moreover, we have demonstrated that VPP-G kills *S. aureus* through both inhibition of cell wall biosynthesis and disruption of the bacterial membrane, a dual mechanism that would prevent *S. aureus* from developing resistance (Figure 1b). Moreover, for the first time, we have demonstrated the excellent *in vivo* anti-MRSA efficacy of CPP-antibiotic conjugate in a mouse bloodstream infection model.

## RESULTS AND DISCUSSION

### Synthesis and Characterization of Conjugate VPP-G.

To synthesize VPP-G, an azido-functionalized backbone  $\text{N}_3$ -PEG-PCHLG ( $\text{N}_3$ -PP) was first synthesized via the ring-opening polymerization (ROP) of *N*-carboxyanhydride (NCA) of  $\gamma$ -(6-chlorohexyl)-*L*-glutamate (CHLG) with  $\text{N}_3$ -PEG-NH<sub>2</sub> (an ethylene glycol oligomer of six units) as the initiator in DMF (Scheme S1, Figure S1). The controlled living NCA-ROP enabled facile synthesis of polypeptides with defined length and low polydispersity (PDI < 1.25).<sup>43,44</sup> The degree of polymerization (DP) was controlled to be  $\sim 10$  to ensure sufficient helicity and membrane activity of the polypeptides while maximizing the weight percentage of antibiotic. This DP was selected based on our preliminary studies, in which polypeptide with a DP of 10 was found to yield the best activity (Figure S10). Monomer CHLG was selected so that the charged guanidinium group will be 16  $\sigma$ -bonds away from

the backbone in the final product. Oligo(ethylene glycol) was used as a flexible linker between vancomycin and CPP so that both can maintain their independent function. Propynyl-functionalized vancomycin was then attached to the backbone  $\text{N}_3$ -PP to yield VPP via copper(I)-catalyzed azide-alkyne cycloaddition (CuAAC) click reaction. Propynyl-vancomycin was synthesized by coupling 2-propynylamine to the carboxyl group of vancomycin (Scheme S3, Figures S2–4). Previous studies have shown that the modification on this carboxyl group minimally impacts the antimicrobial activity of vancomycin,<sup>45,46</sup> which was further confirmed by our antimicrobial test of vancomycin and propynyl-vancomycin (Figure S5). The chloro groups of the side chains of VPP were then converted to azido groups, followed by another CuAAC click reaction to attach the 2-propynylguanidinium to the side chains of polypeptide to yield VPP-G (Scheme S4, Figures S6 and S7). To confirm that the antimicrobial activity of vancomycin was not negatively affected by the reaction condition, free vancomycin was treated in the same way as the conjugated vancomycin, and its antimicrobial activity was found to be similar as that of untreated vancomycin (Figure S5). PP-G, the metaphilic CPP without conjugation of vancomycin, was synthesized as a control (Scheme S5, Figure S8). The molar ratio of PP-G and vancomycin in VPP-G was determined to be 1:1, suggesting that each PP-G has been successfully conjugated with a vancomycin (Figures S6 and S7). VPP-G was found to adopt the characteristic helical conformation in the presence of conjugated vancomycin (Figure S9).

**In Vitro Antimicrobial Activity and Toxicity.** The antimicrobial activity of VPP-G and its controls against both extracellular and intracellular pathogens was first evaluated using RAW 264.7 macrophage and *S. aureus* (ATCC12608) as the model host cell and pathogen, respectively. Consistent with the literature,<sup>14</sup> although vancomycin (Van) shows potent antimicrobial activity against extracellular *S. aureus* (MIC = 0.7  $\mu\text{M}$ ), its activity against intracellular *S. aureus* (IMBC<sub>99,9</sub> > 710  $\mu\text{M}$ ) drastically decreases by 1000 times (Figure 2a and Table 1). In contrast, the conjugate VPP-G exhibits potent antimicrobial activity against both extracellular and intracellular *S. aureus*, with MIC = 3  $\mu\text{M}$  and IMBC<sub>99,9</sub> = 9  $\mu\text{M}$ , respectively. Despite that VPP-G has slightly lower extracellular antibacterial activity than free vancomycin, its activity against intracellular *S. aureus* is >80-fold higher than free vancomycin. Moreover, unlike free vancomycin, whose intracellular antibacterial activity is insensitive to concentration change due to poor membrane permeability, the intracellular antibacterial activity of VPP-G is highly concentration-dependent, suggesting the excellent membrane penetrating capability of VPP-G (Figures 2b and S11). Metaphilic PP-G by itself shows moderate antimicrobial activity (MIC = 66  $\mu\text{M}$ ), but the similar extracellular and intracellular antimicrobial activity indicates its high membrane permeability, as the membrane barrier is unable to drastically decrease its intracellular antimicrobial activity. Interestingly, a 1:1 mixture of vancomycin and PP-G exhibits strong activity against extracellular bacteria (MIC = 0.7  $\mu\text{M}$ ) but weak activity against intracellular bacteria (IMBC<sub>99,9</sub> = 95  $\mu\text{M}$ ) (Figure 2a and b). The extracellular antimicrobial activity is mainly attributed to vancomycin, while the intracellular antimicrobial activity is dominated by PP-G, which suggests that an unconjugated mixture does not facilitate the penetration of molecules as large as vancomycin (1.4 kDa) into host cells.

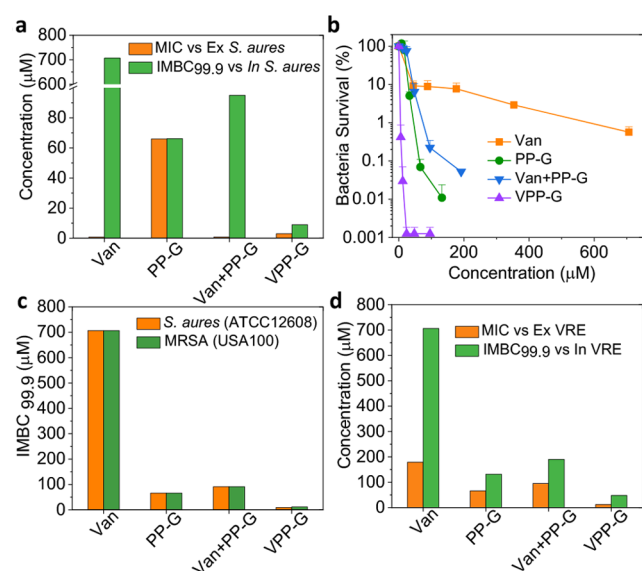


**Figure 2.** *In vitro* antimicrobial activity of VPP-G and its controls. (a) MIC (minimum inhibitory concentration to completely inhibit bacterial growth) against extracellular *S. aureus* (ATCC12608) and the IMBC<sub>99.9</sub> (the minimum bactericidal concentration to kill 99.9% of intracellular bacteria) against intracellular *S. aureus* (ATCC12608) of VPP-G and controls. (b) Survival curve of intracellular *S. aureus* (ATCC12608) after treatment with VPP-G and controls of various concentrations. (c) Comparison of IMBC<sub>99.9</sub> of VPP-G and controls against intracellular *S. aureus* (ATCC12608) and MRSA (USA100). (d) MIC and IMBC<sub>99.9</sub> of VPP-G and controls against extracellular and intracellular VRE (ATCC51858), respectively.

VPP-G also actively kills multidrug-resistant bacterial strains. The intracellular activity of VPP-G against MRSA (USA100) is similar to drug-sensitive *S. aureus* (ATCC12608) (Figure 2c and Figure S11a). To evaluate whether VPP-G is also active against vancomycin-resistant bacteria, we evaluated its antimicrobial activity against vancomycin-resistant *Enterococci* (VRE, ATCC51858) (Figure 2d and Figure S11b). Unlike *S. aureus* and MRSA, both extracellular and intracellular VRE are highly resistant to vancomycin, with MIC = 176  $\mu\text{M}$  and IMBC<sub>99.9</sub> > 710  $\mu\text{M}$ , respectively. Weak antimicrobial activity against both extracellular and intracellular VRE was also found for PP-G and 1:1 mixture of vancomycin and PP-G. Interestingly, in addition to the expected improved activity against intracellular VRE, high activity against extracellular VRE was also observed for VPP-G, though neither of its building blocks (vancomycin and PP-G) show good potency against VRE. This enhanced activity suggests that the conjugated vancomycin and PP-G work synergistically to kill VRE.

The *in vitro* cell toxicity of VPP-G was evaluated by the hemolysis of human red blood cells and the cell viability of

RAW 246.7 macrophages (Table 1, Figure S12a,b). Both PP-G and VPP-G exhibit some membrane-activity-associated cytotoxicity (HC<sub>50</sub>  $\approx$  70–100  $\mu\text{M}$  and IC<sub>50</sub>  $\approx$  100–130  $\mu\text{M}$ , where HC<sub>50</sub> is the minimum concentration to lyse 50% of HRBC and IC<sub>50</sub> is the minimum concentration to kill 50% of RAW 246.7). However, it should be noted that both HC<sub>50</sub> and IC<sub>50</sub> values of VPP-G are 8–11 times higher than its IMBC<sub>99.9</sub> against intracellular *S. aureus* and MRSA (Table 1). At the IMBC<sub>99.9</sub> of VPP-G against intracellular *S. aureus*, macrophages have a viability >90% after treatment with PP-G or VPP-G (Figure S12c–g).

**VPP-G Enters the Cell via Direct Metaphilic Membrane Penetration.** Following the *in vitro* biological activity studies, we investigated the membrane penetration mechanism of VPP-G. VPP-G is designed to be capable of crossing mammalian cell membranes to kill the intracellular bacteria. To confirm its membrane penetration capability, VPP-G was labeled by DBCO-Cy5 via copper-free click reaction (Scheme S6). RAW264.7 macrophages treated with Cy5-VPP-G of different concentrations were imaged under confocal microscopy (Figure 3a). Cy5-VPP-G actively penetrates into macrophages and the intracellular Cy5-VPP-G concentration increases with the increase of feed concentration. At low concentration, Cy5-VPP-G is mostly found in the cytosol. However, as the feed concentration increases, Cy5-VPP-G diffuses throughout the entire cytosol and eventually distributes everywhere inside the cell, including the nucleus. The relative mean fluorescent intensity (MFI) of intracellular Cy5-VPP-G to Hoechst correlates almost linearly with Cy5-VPP-G feed concentration ( $R^2 = 0.979$ ) at the tested concentration range (Figure 3b), suggesting that VPP-G diffuses freely across the cell membrane.

To elucidate whether VPP-G enters the cell via direct membrane penetration or endocytosis, we stained the RAW264.7 cells using LysoTracker, with or without Cy5-VPP-G pretreatment (Figure 3c). LysoTracker nonselectively stains cells regardless of whether they are treated with Cy5-VPP-G or not, but only those treated with Cy5-VPP-G exhibit a bright Cy5 fluorescence throughout the cell (Figures 3c and S13a,c). Most Cy5 fluorescence is noted not to overlap with the lysosomes, suggesting that VPP-G enters the cell primarily via direct membrane penetration, similar to the behavior of metaphilic CPPs reported previously.<sup>38</sup> To further determine whether VPP-G is able to locate intracellular bacteria, RAW 264.7 cells were first infected with SYTO9-stained *S. aureus* and then either treated with Cy5-VPP-G or not. Almost all the SYTO9-stained *S. aureus* are found to be colocalized with Cy5-VPP-G (Figure 3d). While all cells contain SYTO9-labeled *S. aureus*, only cells treated with Cy5-VPP-G exhibit strong Cy5 fluorescence (Figures 3d and S13b,d). It should be noted that the MFI of SYTO9 is weaker for cells treated with VPP-G than

**Table 1.** Summary of the *In Vitro* Antimicrobial Activity and Cytotoxicity of Vancomycin, PP-G, and VPP-G

samples	extracellular MIC ( $\mu\text{M}$ )			intracellular IMBC <sub>99.9</sub> ( $\mu\text{M}$ )			IC <sub>50</sub> ( $\mu\text{M}$ )	HC <sub>50</sub> ( $\mu\text{M}$ )	IC <sub>50</sub> /IMBC <sub>99.9</sub>		
	SA <sup>a</sup>	MRSA <sup>b</sup>	VRE <sup>c</sup>	SA	MRSA	VRE	RAW <sup>d</sup>	RBC <sup>e</sup>	SA	MRSA	VRE
Van	0.69	0.69	176	>706	>706	>706	>706	>1412	$\geq 1$	$\geq 1$	$\geq 1$
PP-G	66	66	66	66	66	132	132	66	2	2	1
V+PP-G	0.74	0.74	95	95	95	190	N.T.	N.T.	/	/	/
VPP-G	3.0	3.0	12	9.0	12	48	96	96	11	8	2

<sup>a</sup>*S. aureus* (ATCC12608). <sup>b</sup>MRSA (USA100). <sup>c</sup>VRE (ATCC51858). <sup>d</sup>RAW264.7; <sup>e</sup>Human red blood cell; N.T.: not tested.

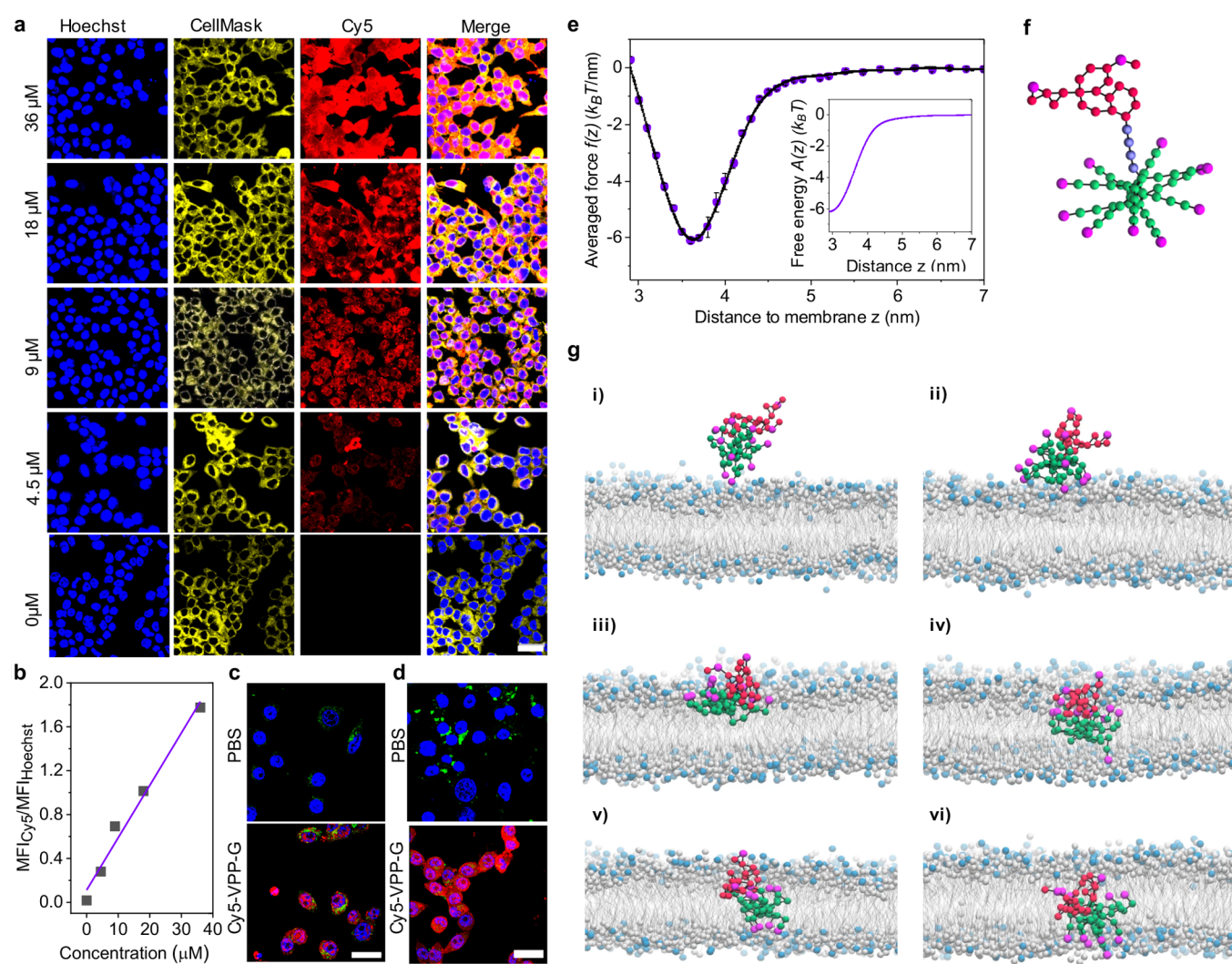


**Figure 3.** Cellular internalization and membrane penetration of VPP-G. (a) Confocal images of RAW264.7 macrophages treated with Cy5-VPP-G of various concentrations. Blue: Hoechst; yellow: CellMask; red: Cy5-VPP-G. Scale bar: 20  $\mu\text{m}$ . (b) Relative mean fluorescence intensity (MFI) of intracellular Cy5-VPP-G to Hoechst as a function of Cy5-VPP-G feed concentration. Data points were fitted linearly ( $R^2 = 0.979$ ). (c) Confocal images of RAW264.7 cells stained with Lysotracker, with and without Cy5-VPP-G pretreatment (9  $\mu\text{M}$ ). Blue: Hoechst; green: Lysotracker; red: Cy5-VPP-G. Scale bar: 20  $\mu\text{m}$ . (d) Confocal images of *S. aureus*-infected RAW264.7 cells with and without Cy5-VPP-G treatment (9  $\mu\text{M}$ ). *S. aureus* was stained with SYTO9 before infection. Blue: Hoechst; green: SYTO9; red: Cy5-VPP-G. Scale bar: 20  $\mu\text{m}$ . (e) Time-averaged force  $f(z)$  exerted on VPP-G approaching a lipid membrane (20% anionic lipids). The force is evaluated as a function of the distance  $z$  between the mass center of VPP-G and the head groups of the membrane outer leaflet. Inset shows the free-energy  $A(z)$  profile, obtained through integration of the force profile  $f(z)$ . (f) Conformation of VPP-G in free solution. (g) Simulation images demonstrating the landing (i), anchoring (ii), submersion (iii), initial tunneling (iv, in which a charged side chain reaches the inner leaflet), membrane-spanning (v), and full insertion (vi) of VPP-G. Surrounding ions and water molecules are not shown. Green beads: hydrophobic components of polypeptides; purple beads: positively charged groups; red beads: vancomycin; cyan beads: negatively charged lipid heads; gray beads: zwitterionic lipid heads. Each bead has the size of a lipid head (diameter  $\sigma = 8.5 \text{ \AA}$ ).

cells treated with PBS, suggesting some of the intracellular *S. aureus* have been killed by VPP-G.

To further illustrate how VPP-G enters the cell, we performed generic coarse-grained molecular dynamics (MD) simulations. We first used a steered MD simulation to track the force and energy change as VPP-G approaches a lipid membrane (composed of 20% negatively charged lipids and 80% zwitterionic lipids) in aqueous environment. At large separation ( $z > 6 \text{ nm}$ , defined as the distance between the mass center of VPP-G and the membrane surface of the outer leaflet), VPP-G barely senses the oppositely charged membrane due to electrostatic screening by the ions (Figure 3e). As it diffuses closer to the membrane, an attractive force  $f(z)$  emerges at  $z < 6 \text{ nm}$  and reaches a maximum around 3.6

nm. This electrostatic attraction results in a  $6.1k_B T$  reduction in free energy  $A(z)$  upon binding to the membrane surface (inset of Figure 3e), which provides a sufficient driving force for the landing process of VPP-G. We then simulated the landing and membrane insertion process of VPP-G. Consistent with what we previously reported,<sup>38</sup> VPP-G employs a metaphilic membrane-penetration mechanism to cross the lipid bilayer. In free solution, VPP-G is represented as an extended vancomycin attached to a radially amphiphilic helical CPP via a PEG linker (Figure 3f). When interacting with the lipid membrane, VPP-G first lands with its positively charged side chains on the negatively charged membrane (Figure 3g(i)). Once the landing has been initiated, more of the cationic side chains reorganize to one face to enhance the

membrane anchoring process (Figure 3g(ii)). The hydrophobic effect then drives the exposed hydrophobic face of VPP-G to submerge into the hydrophobic domain of the lipid bilayer (Figure 3g(iii)). Due to the matching lengths of the polypeptide side chains and the lipid tails, the cationic side chains “tunnel” from the outer leaflet to the inner leaflet (Figure 3g(iv)). As more side chains reach the inner leaflet, VPP-G spans across the lipid bilayer, which is followed by full membrane insertion (Figure 3g(v) and (vi), respectively). We note that in an actual mammalian plasma membrane, the inner leaflet carries more negatively charged lipids than the outer leaflet, which provides an additional driving force for membrane penetration. The metaphilic membrane-penetration mechanism described here efficiently transports hydrophilic antibiotics as large as vancomycin (1449 Da) into the host cells and, to the best of our knowledge, has not been reported for other CPPs based on short side chains.

**VPP-G Kills Bacteria via a Dual Antimicrobial Mechanism.** Vancomycin is known to kill bacteria by inhibiting cell wall biosynthesis.<sup>47,48</sup> Because PP-G is membrane-active, VPP-G was predicted to have a dual antimicrobial mechanism. We have already demonstrated that VPP-G is much more active than PP-G, possibly because of the cell wall biosynthesis inhibitory activity of conjugated vancomycin. In this work, we used scanning electron microscopy (SEM) to confirm the cell wall biosynthesis inhibitory activity of VPP-G (Figure 4a). *S. aureus* cells treated

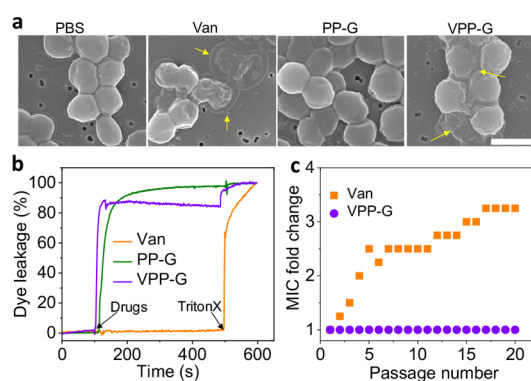


**Figure 4.** Dual antimicrobial mechanism and drug resistance of VPP-G. (a) SEM images of *S. aureus* (ATCC12608) treated with PBS, Van, PP-G, and VPP-G. Scale bar: 1  $\mu$ m. (b) Dye leakage profile from liposomes (DOPG/cardioliipin = 50/50) treated with VPP-G (9  $\mu$ M), PP-G (9  $\mu$ M), and Van (9  $\mu$ M). Drugs (Van, PP-G, and VPP-G) were added at  $t \sim 100$  s, while TritonX-100 was added at  $t \sim 500$  s to completely lyse the liposomes and yield 100% leakage. (c) Resistance induction of vancomycin and VPP-G as indicated by the passage number and change in MICs.

by PBS and PP-G have an intact cell wall, indicating that PP-G by itself does not inhibit cell wall biosynthesis. However, *S. aureus* cells treated with vancomycin exhibit a damaged bacterial cell wall, with some of the bacterial cells completely collapsed (depicted by arrows in Figure 4a), which may due to the weakened mechanical strength of the damaged cell walls. Similarly, *S. aureus* cells treated with VPP-G also present damaged cell walls and collapsed cells, indicating that VPP-G inhibits cell wall biosynthesis as well. Previous studies have also reported that the conjugation of a cationic peptide to the carboxylic group of vancomycin impact minimally on the binding site of conjugated vancomycin to its target.<sup>45,46</sup>

We further used a liposome model to validate that VPP-G disrupts bacterial membrane (Figure 4b). Liposomes composed of DOPG/cardioliipin = 50/50 were prepared to mimic the membrane composition of *S. aureus*.<sup>49</sup> Dye 5(6)-carboxy-fluorescein, which quenches itself at concentration >40 mM,<sup>50</sup> was incorporated into the liposomes, and the dye leakage profile before and after the addition of VPP-G was recorded as a function of time. While vancomycin shows no membrane activity, both PP-G and VPP-G clearly disrupt the liposome membrane, as evidenced by the complete dye leakage upon the addition of VPP-G or PP-G. Furthermore, by determining the percentage of dye leakage at various concentrations, we confirmed that VPP-G and PP-G have similar membrane activity (Figure S14a). The similarity in membrane activity indicates that the enhanced antimicrobial activity and the cell wall inhibition activity of VPP-G contribute to the engagement of conjugated vancomycin with its target. More importantly, this membrane disruption activity is much weaker against human cell membrane (Figure S14b), as indicated by the low dye leakage from liposomes (DOPC/cholesterol = 60/40) mimicking mammalian membranes.<sup>51</sup> This selectivity is due to the difference in lipid composition between bacterial and mammalian membranes and is consistent with the behavior of many other membrane-active antimicrobials.<sup>52–54</sup>

Because of this dual antimicrobial mechanism, VPP-G is predicted to prevent bacteria from developing drug resistance. To confirm this, we performed a resistance test by serially passing bacteria exposed to subinhibitory concentrations of vancomycin or VPP-G. Significantly, resistance to VPP-G was not observed over the course of 20 passages (Figure 4c). In contrast, resistance to vancomycin developed rapidly, with MIC doubling within 5 passages and tripling after 20 passages. Enabled by this dual antimicrobial mechanism, VPP-G is also expected to be capable of killing dormant intracellular bacteria, as previous studies have demonstrated that membrane-active antimicrobial peptides with fast killing kinetics can kill persistent and dormant bacteria.<sup>55,56</sup>

**VPP-G Efficiently Eradicates MRSA *In Vivo* in a Mouse Intravenous Infection Model.** Although several different types of CPP–antibiotic conjugates have been developed to eradicate intracellular pathogens, studies on *in vivo* antimicrobial efficacy in animal models have been reported only infrequently and have achieved very limited success.<sup>24,27,57</sup> In this work, we adopted a mouse intravenous infection model to demonstrate the *in vivo* antimicrobial efficacy of VPP-G against MRSA. This model has been previously used to study the *in vivo* efficacy of antibody–drug conjugates against intracellular MRSA by Genentech.<sup>4</sup> The process of bacterial infection and drug administration is shown in Figure 5a. MRSA (USA100,  $2 \times 10^7$  CFU) was inoculated intravenously through tail vein injection. Vancomycin (100 mg/kg), VPP-G (72 mg/kg,  $1.5 \times \text{IMBC}_{99,9}$ ), and PP-G (50 mg/kg, mole number equivalent to VPP-G) were administered via intraperitoneal injection. The first dose was given 24 h after infection to ensure enough cellular uptake and proliferation of MRSA.<sup>4</sup> The concentration of vancomycin injected was 2 times of its serum  $C_{\text{max}}$  ( $\sim 50$  mg/L by previous studies<sup>58</sup>). Major organs were collected and homogenized for CFU determination (Figure 5b,c, Figure S15). Consistent with earlier reports,<sup>4</sup> vancomycin is capable of reducing the kidney bacterial burden by  $\sim 10^2$ -fold (Figure 5b). The survived bacteria are mostly those hidden inside of cells.<sup>4</sup> On the other hand, VPP-G is able to reduce bacterial burden by  $10^3$ – $10^4$ -fold (Figure 5b,c), which is significantly

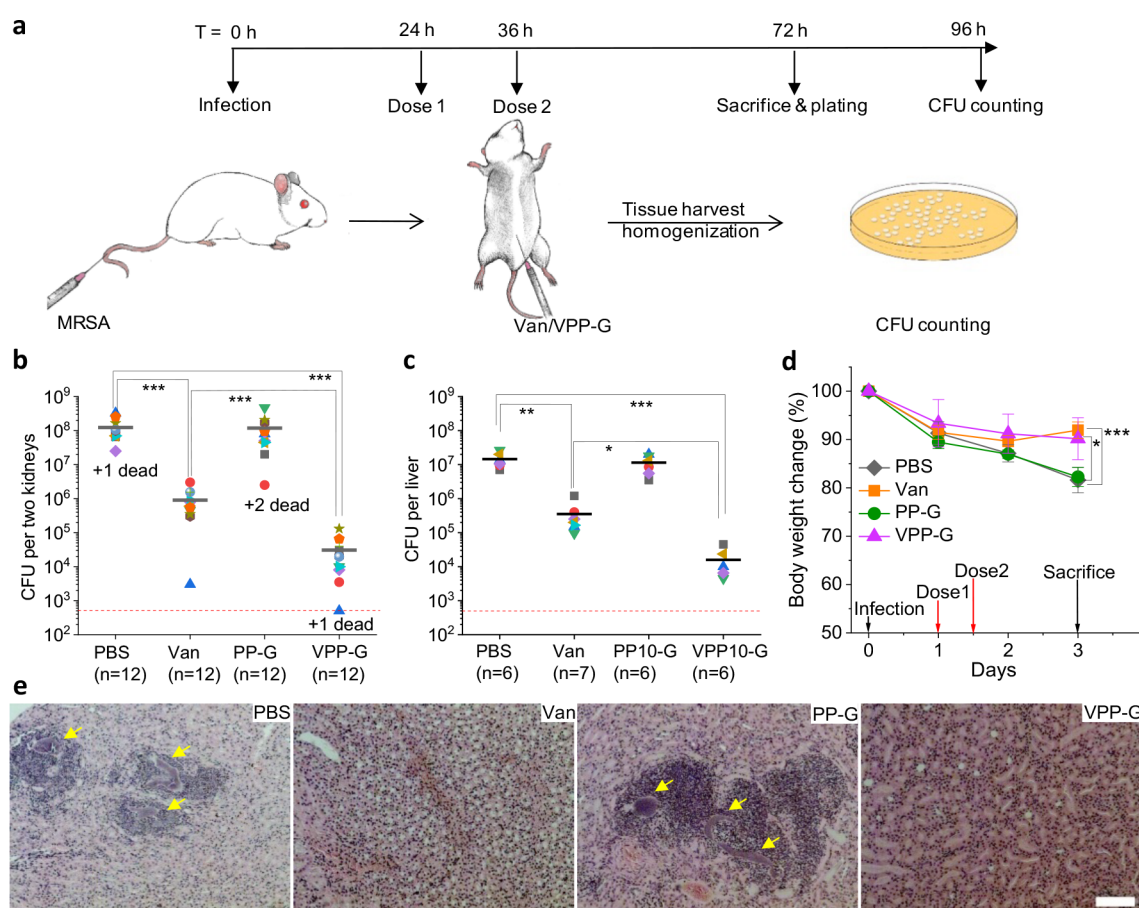


**Figure 5.** *In vivo* antimicrobial activity of VPP-G in a mouse intravenous MRSA infection model. (a) Schematic representation of the *in vivo* study. Mice were infected with MRSA (USA 100,  $2 \times 10^7$  CFU) at  $T = 0$  h and treated with PBS, vancomycin (100 mg/kg), VPP-G (72 mg/kg,  $1.5 \times \text{MBC}_{99.9}$ ), and PP-G (50 mg/kg, molar equivalent to VPP-G) at  $T = 24$  and 36 h. Mice were sacrificed at  $T = 72$  h and major organs (kidney, liver, spleen, and heart) were collected for bacterial burden determination and histology analysis. The bacterial burden of kidneys (b) and liver (c) from MRSA-infected mice treated with PBS, vancomycin, PP-G, and VPP-G. Red dotted line indicates the detection limit. (d) Body weight of MRSA-infected mice treated with PBS, vancomycin, PP-G, and VPP-G. For (b–d): \*  $P < 0.05$ , \*\*  $P < 0.01$ , \*\*\*  $P < 0.005$ . (e) H&E staining of kidney from MRSA-infected mice treated with PBS, vancomycin, PP-G, and VPP-G. Scale bar: 500  $\mu\text{m}$ .

more active than vancomycin, suggesting that VPP-G kills not only extracellular bacteria, but also intracellular ones. The same amount of PP-G is unable to significantly reduce the bacterial burden (Figure 5b,c), which is consistent with the relatively low *in vitro* antimicrobial activity of PP-G by itself. A similar trend is also found for the bacterial burden in the liver and spleen, but is less obvious in the heart, since the low bacterial burden in the heart is close to the detection limit (Figure 5c, Figure S15).

The *in vivo* therapeutic efficacy was further confirmed by body weight and histopathological changes. Mice treated with vancomycin and VPP-G stopped losing body weight after the second dose and some of them started to gain weight by day 3 (Figure 5d). However, mice treated with PP-G and PBS continued to lose weight. The kidney histology analysis further supports the *in vivo* efficacy of VPP-G (Figure 5e). For PBS and PP-G treated mice, the kidneys were characterized with the presence of granulomatous foci, a typical structure formed during infection and inflammation when the immune system attempts to wall off infectious substances. Bacterial-associated inflammatory responses, such as infiltration of immune cells and renal tubular necrosis, were observed as well (Table S1). In contrast, the kidneys of mice treated with vancomycin and VPP-G exhibited almost no granulomatous foci. However, for

the VPP-G treated group, a mild to moderate degree of neutrophil infiltration and renal tubular necrosis were observed (Table S1), although the level is significantly lower than for the PBS-treated group, which could be caused by toxicity associated with the metaphilic CPP.

## CONCLUSION

In summary, we have developed a metaphilic CPP–antibiotic conjugate VPP-G, which can effectively eradicate >99.9% of both extracellular and intracellular pathogens, including *S. aureus*, MRSA, and VRE. It diffuses into the host cell via a unique metaphilic membrane-penetration mechanism to tackle intracellular bacteria. VPP-G kills bacteria through a dual antimicrobial mechanism: inhibition of cell wall biosynthesis and disruption of the bacterial membrane. This dual mechanism prevents the bacteria from developing resistance and offers potentially additional advantages of killing dormant intracellular bacteria that are resistant to conventional antibiotics. We also demonstrated that VPP-G can effectively eradicate MRSA in a mouse intravenous infection model, outperforming high concentrations of vancomycin. With the widespread threats of infectious diseases caused by intracellular bacteria and the growing antibiotic drug resistance, the conjugates of antibiotics with a remarkably membrane-active,

adaptive, metaphilic CPP may provide alternative solutions to these concerns.

## ■ ASSOCIATED CONTENT

### SI Supporting Information

The Supporting Information is available free of charge at <https://pubs.acs.org/doi/10.1021/acscentsci.0c00893>.

Materials, methods, and experimental procedures, including compound synthesis, *in vitro* activity and toxicity, as well as *in vivo* activity and toxicity. Supplementary figures showing the structural characterizations, *in vitro* activity and toxicity, mechanistic studies, and *in vivo* anti-MRSA efficacy and histology analysis (PDF)

## ■ AUTHOR INFORMATION

### Corresponding Authors

**Erik Luijten** – Department of Materials Science and Engineering, Department of Engineering Sciences and Applied Mathematics, Department of Chemistry, and Department of Physics and Astronomy, Northwestern University, Evanston, Illinois 60208, United States; [orcid.org/0000-0003-2364-1866](https://orcid.org/0000-0003-2364-1866); Email: [luijten@northwestern.edu](mailto:luijten@northwestern.edu)

**Jianjun Cheng** – Department of Materials Science and Engineering, Beckman Institute for Advanced Science and Technology, Department of Bioengineering, and Department of Chemistry, University of Illinois at Urbana–Champaign, Urbana, Illinois 61801, United States; [orcid.org/0000-0003-2561-9291](https://orcid.org/0000-0003-2561-9291); Email: [jianjunc@illinois.edu](mailto:jianjunc@illinois.edu)

### Authors

**Yunjiang Jiang** – Department of Materials Science and Engineering and Beckman Institute for Advanced Science and Technology, University of Illinois at Urbana–Champaign, Urbana, Illinois 61801, United States

**Ming Han** – Applied Physics Graduate Program, Northwestern University, Evanston, Illinois 60208, United States; Chicago Materials Research Center, University of Chicago, Chicago, Illinois 60637, United States; [orcid.org/0000-0002-9108-8364](https://orcid.org/0000-0002-9108-8364)

**Yang Bo** – Department of Materials Science and Engineering, University of Illinois at Urbana–Champaign, Urbana, Illinois 61801, United States

**Yujun Feng** – Department of Materials Science and Engineering, University of Illinois at Urbana–Champaign, Urbana, Illinois 61801, United States

**Wenming Li** – Department of Materials Science and Engineering, University of Illinois at Urbana–Champaign, Urbana, Illinois 61801, United States

**Jason Ren Wu** – Department of Bioengineering, University of Illinois at Urbana–Champaign, Urbana, Illinois 61801, United States

**Ziyuan Song** – Department of Materials Science and Engineering, University of Illinois at Urbana–Champaign, Urbana, Illinois 61801, United States; [orcid.org/0000-0002-3165-3712](https://orcid.org/0000-0002-3165-3712)

**Zihao Zhao** – Department of Materials Science and Engineering, University of Illinois at Urbana–Champaign, Urbana, Illinois 61801, United States

**Zhengzhong Tan** – Department of Materials Science and Engineering, University of Illinois at Urbana–Champaign, Urbana, Illinois 61801, United States

**Yingying Chen** – Department of Materials Science and Engineering, University of Illinois at Urbana–Champaign, Urbana, Illinois 61801, United States

**Tianrui Xue** – Department of Chemistry, University of Illinois at Urbana–Champaign, Urbana, Illinois 61801, United States

**Zihuan Fu** – Department of Chemistry, University of Illinois at Urbana–Champaign, Urbana, Illinois 61801, United States

**Shanny Hsuan Kuo** – Department of Pathobiology, University of Illinois at Urbana–Champaign, Urbana, Illinois 61801, United States

**Gee W. Lau** – Department of Pathobiology, University of Illinois at Urbana–Champaign, Urbana, Illinois 61801, United States

Complete contact information is available at:

<https://pubs.acs.org/doi/10.1021/acscentsci.0c00893>

### Author Contributions

Y.J. and J.C. conceived and designed the project and wrote the paper. Y.J., Y.B., Y.F., and J.W. performed the experiments. W.L. helped with the vancomycin modification, Z.S. contributed discussions on the polypeptide synthesis. G.L. and H.K. assisted with the histology analysis. M.H. and E.L. performed the molecular dynamic simulations and data analysis. All authors discussed the data and commented on the manuscript.

### Notes

The authors declare no competing financial interest.

## ■ ACKNOWLEDGMENTS

J.C. and E.L. acknowledge funding support from the National Science Foundation (CHE-1709820 for J.C. and DMR-1610796 for E.L.). This project was also partially supported by an NIH grant (1R01CA207584, J.C.). We acknowledge the facility and instrumental support from the Illinois Materials Research Laboratory, the NMR Laboratory of the School of Chemical Sciences, the Carl R. Woese Institute for Genomic Biology, and the Beckman Institute for Advanced Science and Technology, at University of Illinois at Urbana–Champaign.

## ■ REFERENCES

- (1) Brown, A. E.; Leech, J. M.; Rogers, T. R.; McLoughlin, R. M. Staphylococcus aureus colonization: modulation of host immune response and impact on human vaccine design. *Front. Immunol.* **2014**, *4*, 1 DOI: [10.3389/fimmu.2013.00507](https://doi.org/10.3389/fimmu.2013.00507).
- (2) Lowy, F. D. Medical progress - Staphylococcus aureus infections. *N. Engl. J. Med.* **1998**, *339* (8), 520–532.
- (3) Kourtis, A. P.; Hatfield, K.; Baggs, J.; Mu, Y.; See, I.; Epton, E.; Nadle, J.; Kainer, M. A.; Dumyati, G.; Petit, S.; Ray, S. M.; Ham, D.; Capers, C.; Ewing, H.; Coffin, N.; McDonald, L. C.; Jernigan, J.; Cardo, D.; Program, E. I. Vital Signs: Epidemiology and Recent Trends in Methicillin-Resistant and in Methicillin-Susceptible Staphylococcus aureus Bloodstream Infections- United States. *Morbidity and Mortality Weekly Report* **2019**, *68* (9), 214–219.
- (4) Lehar, S. M.; Pillow, T.; Xu, M.; Staben, L.; Kajihara, K. K.; Andlen, R. V.; DePalatis, L.; Raab, H.; Hazenbos, W. L.; Morisaki, J. H.; Kim, J.; Park, S.; Darwish, M.; Lee, B. C.; Hernandez, H.; Loyet, K. M.; Lupardus, P.; Fong, R. N.; Yan, D.; Halouni, C. C.; Luis, E.; Khalif, Y.; Plise, E.; Heong, J. C.; Lyssikatos, J. P.; Strandh, M.; Koefoed, K.; Andersen, P. S.; Flygare, J. A.; Tan, M. W.; Brown, E. J.; Ariathasan, S. M. Novel antibody-antibiotic conjugate eliminates intracellular *S. aureus*. *Nature* **2015**, *527* (7578), 323–328.
- (5) Rollin, G.; Tan, X.; Tros, F.; Dupuis, M.; Nassif, X.; Charbit, A.; Coureuil, M. Intracellular Survival of Staphylococcus aureus in

Endothelial Cells: A Matter of Growth or Persistence. *Front. Microbiol.* **2017**, *8*, 1 DOI: 10.3389/fmicb.2017.01354.

(6) Garzoni, C.; Kelley, W. L. Staphylococcus aureus: new evidence for intracellular persistence. *Trends Microbiol.* **2009**, *17* (2), 59–65.

(7) Bo, Y.; Jiang, Y.; Chen, K.; Cai, K.; Li, W.; Roy, J.; Bao, Y.; Cheng, J. Targeting infected host cells in vivo via responsive azido-sugar mediated metabolic cell labeling followed by click reaction. *Biomaterials* **2020**, *238*, 119843–119854.

(8) Brouillette, E.; Grondin, G.; Shkreta, L.; Lacasse, P.; Talbot, B. G. In vivo and in vitro demonstration that Staphylococcus aureus is an intracellular pathogen in the presence or absence of fibronectin-binding proteins. *Microb. Pathog.* **2003**, *35* (4), 159–168.

(9) Fraunholz, M.; Sinha, B. Intracellular Staphylococcus aureus: live-in and let die. *Front. Cell. Infect. Microbiol.* **2012**, *2*, 43.

(10) Jarry, T. M.; Memmi, G.; Cheung, A. L. The expression of alpha-haemolysin is required for Staphylococcus aureus phagosomal escape after internalization in CFT-1 cells. *Cell. Microbiol.* **2008**, *10* (9), 1801–1814.

(11) Uribe-Querol, E.; Rosales, C. Control of Phagocytosis by Microbial Pathogens. *Front. Immunol.* **2017**, *8*, 1 DOI: 10.3389/fimmu.2017.01368.

(12) Thakur, A.; Mikkelsen, H.; Jungersen, G. Intracellular Pathogens: Host Immunity and Microbial Persistence Strategies. *J. Immunol. Res.* **2019**, *2019*, 1.

(13) Monack, D. M.; Mueller, A.; Falkow, S. Persistent bacterial infections: The interface of the pathogen and the host immune system. *Nat. Rev. Microbiol.* **2004**, *2* (9), 747–765.

(14) Darouiche, R. O.; Hamill, R. J. Antibiotic Penetration of and Bactericidal Activity within Endothelial-Cells. *Antimicrob. Agents Chemother.* **1994**, *38* (5), 1059–1064.

(15) Seral, C.; Van Bambeke, F.; Tulkens, P. M. Quantitative analysis of gentamicin, azithromycin, telithromycin, ciprofloxacin, moxifloxacin, and oritavancin (LY333328) activities against intracellular Staphylococcus aureus in mouse J774 macrophages. *Antimicrob. Agents Chemother.* **2003**, *47* (7), 2283–2292.

(16) Baltch, A. L.; Ritz, W. J.; Bopp, L. H.; Michelsen, P. B.; Smith, R. P. Antimicrobial activities of daptomycin, vancomycin, and oxacillin in human monocytes and of daptomycin in combination with gentamicin and/or rifampin in human monocytes and in broth against Staphylococcus aureus. *Antimicrob. Agents Chemother.* **2007**, *51* (4), 1559–1562.

(17) Barcia-Macay, M.; Seral, C.; Mingeot-Leclercq, M. P.; Tulkens, P. M.; Van Bambeke, F. Pharmacodynamic evaluation of the intracellular activities of antibiotics against Staphylococcus aureus in a model of THP-1 macrophages. *Antimicrob. Agents Chemother.* **2006**, *50* (3), 841–851.

(18) Sandberg, A.; Hessler, J. H. R.; Skov, R. L.; Blom, J.; Fridtjof-Moeller, N. Intracellular Activity of Antibiotics against Staphylococcus aureus in a Mouse Peritonitis Model. *Antimicrob. Agents Chemother.* **2009**, *53* (5), 1874–1883.

(19) Yang, S.; Han, X.; Yang, Y.; Qiao, H.; Yu, Z.; Liu, Y.; Wang, J.; Tang, T. Bacteria-Targeting Nanoparticles with Microenvironment-Responsive Antibiotic Release To Eliminate Intracellular Staphylococcus aureus and Associated Infection. *ACS Appl. Mater. Interfaces* **2018**, *10* (17), 14299–14311.

(20) Gao, F.; Xu, L.; Yang, B.; Fan, F.; Yang, L. Kill the Real with the Fake: Eliminate Intracellular Staphylococcus aureus Using Nanoparticle Coated with Its Extracellular Vesicle Membrane as Active-Targeting Drug Carrier. *ACS Infect. Dis.* **2019**, *5* (2), 218–227.

(21) Surewaard, B. G. J.; Deniset, J. F.; Zemp, F. J.; Amrein, M.; Otto, M.; Conly, J.; Omri, A.; Yates, R. M.; Kubes, P. Identification and treatment of the Staphylococcus aureus reservoir in vivo. *J. Exp. Med.* **2016**, *213* (7), 1141–1151.

(22) Xiong, M.; Bao, Y.; Yang, X.; Wang, Y.; Sun, B.; Wang, J. Lipase-Sensitive Polymeric Triple-Layered Nanogel for “On-Demand” Drug Delivery. *J. Am. Chem. Soc.* **2012**, *134* (9), 4355–4362.

(23) Huh, A. J.; Kwon, Y. J. Nanoantibiotics: A new paradigm for treating infectious diseases using nanomaterials in the antibiotics resistant era. *J. Controlled Release* **2011**, *156* (2), 128–145.

(24) Brezden, A.; Mohamed, M. F.; Nepal, M.; Harwood, J. S.; Kuriakose, J.; Seleem, M. N.; Chmielewski, J. Dual Targeting of Intracellular Pathogenic Bacteria with a Cleavable Conjugate of Kanamycin and an Antibacterial Cell-Penetrating Peptide. *J. Am. Chem. Soc.* **2016**, *138* (34), 10945–10949.

(25) Peeler, D. J.; Thai, S. N.; Cheng, Y.; Horner, P. J.; Sellers, D. L.; Pun, S. H. pH-sensitive polymer micelles provide selective and potentiated lytic capacity to venom peptides for effective intracellular delivery. *Biomaterials* **2019**, *192*, 235–244.

(26) Wang, Y.; Cheetham, A. G.; Angacian, G.; Su, H.; Xie, L.; Cui, H. Peptide-drug conjugates as effective prodrug strategies for targeted delivery. *Adv. Drug Delivery Rev.* **2017**, *110*, 112–126.

(27) Lei, E.; Pereira, M. P.; Kelley, S. O. Tuning the Intracellular Bacterial Targeting of Peptidic Vectors. *Angew. Chem., Int. Ed.* **2013**, *52* (37), 9660–9663.

(28) Pereira, M. P.; Shi, J.; Kelley, S. O. Peptide Targeting of an Antibiotic Prodrug toward Phagosome-Entrapped Mycobacteria. *ACS Infect. Dis.* **2015**, *1* (12), 586–592.

(29) Samuel, B. U.; Hearn, B.; Mack, D.; Wender, P.; Rothbard, J.; Kirisits, M. J.; Mui, E.; Wernimont, S.; Roberts, C. W.; Muench, S. P.; Rice, D. W.; Prigge, S. T.; Law, A. B.; McLeod, R. Delivery of antimicrobials into parasites. *Proc. Natl. Acad. Sci. U. S. A.* **2003**, *100* (24), 14281–14286.

(30) Gomasasca, M.; Martins, T. F. C.; Greune, L.; Hardwidge, P. R.; Schmidt, M. A.; Ruter, C. Bacterium-Derived Cell-Penetrating Peptides Deliver Gentamicin To Kill Intracellular Pathogens. *Antimicrob. Agents Chemother.* **2017**, *61* (4), 1 DOI: 10.1128/AAC.02545-16.

(31) Kauffman, W. B.; Fuselier, T.; He, J.; Wimley, W. C. Mechanism Matters: A Taxonomy of Cell Penetrating Peptides. *Trends Biochem. Sci.* **2015**, *40* (12), 749–764.

(32) Allolio, C.; Magarkar, A.; Jurkiewicz, P.; Baxova, K.; Javanainen, M.; Mason, P. E.; Sachl, R.; Cebecauer, M.; Hof, M.; Horinek, D.; Heinz, V.; Rachel, R.; Ziegler, C. M.; Schrofel, A.; Jungwirth, P. Arginine-rich cell-penetrating peptides induce membrane multi-lamellarity and subsequently enter via formation of a fusion pore. *Proc. Natl. Acad. Sci. U. S. A.* **2018**, *115* (47), 11923–11928.

(33) Sgolastra, F.; Deronde, B. M.; Sarapas, J. M.; Som, A.; Tew, G. N. Designing Mimics of Membrane Active Proteins. *Acc. Chem. Res.* **2013**, *46* (12), 2977–2987.

(34) Tang, H.; Yin, L.; Kim, K. H.; Cheng, J. Helical poly(arginine) mimics with superior cell-penetrating and molecular transporting properties. *Chem. Sci.* **2013**, *4* (10), 3839–3844.

(35) Zhang, R.; Zheng, N.; Song, Z.; Yin, L.; Cheng, J. The effect of side-chain functionality and hydrophobicity on the gene delivery capabilities of cationic helical polypeptides. *Biomaterials* **2014**, *35* (10), 3443–3454.

(36) Gabrielson, N. P.; Lu, H.; Yin, L.; Li, D.; Wang, F.; Cheng, J. Reactive and Bioactive Cationic  $\alpha$ -Helical Polypeptide Template for Nonviral Gene Delivery. *Angew. Chem., Int. Ed.* **2012**, *51* (5), 1143–1147.

(37) Yin, L.; Song, Z.; Kim, K. H.; Zheng, N.; Gabrielson, N. P.; Cheng, J. Non-Viral Gene Delivery via Membrane-Penetrating, Mannose-Targeting Supramolecular Self-Assembled Nanocomplexes. *Adv. Mater.* **2013**, *25* (22), 3063–3070.

(38) Lee, M. W.; Han, M.; Bossa, G. V.; Snell, C.; Song, Z.; Tang, H.; Yin, L.; Cheng, J.; May, S.; Luijten, E.; Wong, G. C. L. Interactions between Membranes and “Metaphilic” Polypeptide Architectures with Diverse Side-Chain Populations. *ACS Nano* **2017**, *11* (3), 2858–2871.

(39) Lu, H.; Wang, J.; Bai, Y.; Lang, J.; Liu, S.; Lin, Y.; Cheng, J. Ionic polypeptides with unusual helical stability. *Nat. Commun.* **2011**, *2*, 1 DOI: 10.1038/ncomms1209.

(40) Xiong, M.; Lee, M. W.; Mansbach, R. A.; Song, Z.; Bao, Y.; Peek, R. M.; Yao, C.; Chen, L.; Ferguson, A. L.; Wong, G. C. L.;

Cheng, J. Helical antimicrobial polypeptides with radial amphiphilicity. *Proc. Natl. Acad. Sci. U. S. A.* **2015**, *112* (43), 13155–13160.

(41) Xiong, M.; Bao, Y.; Xu, X.; Wang, H.; Han, Z.; Wang, Z.; Liu, Y.; Huang, S.; Song, Z.; Chen, J.; Peek, R. M.; Yin, L.; Chen, L.; Cheng, J. Selective killing of *Helicobacter pylori* with pH-responsive helix-coil conformation transitionable antimicrobial polypeptides. *Proc. Natl. Acad. Sci. U. S. A.* **2017**, *114* (48), 12675–12680.

(42) Xiong, M.; Han, Z.; Song, Z.; Yu, J.; Ying, H.; Yin, L.; Cheng, J. Bacteria-Assisted Activation of Antimicrobial Polypeptides by a Random-Coil to Helix Transition. *Angew. Chem., Int. Ed.* **2017**, *56* (36), 10826–10829.

(43) Deming, T. J. Living polymerization of alpha-amino acid-N-carboxyanhydrides. *J. Polym. Sci., Part A: Polym. Chem.* **2000**, *38* (17), 3011–3018.

(44) Song, Z.; Han, Z.; Lv, S.; Chen, C.; Chen, L.; Yin, L.; Cheng, J. Synthetic polypeptides: from polymer design to supramolecular assembly and biomedical application. *Chem. Soc. Rev.* **2017**, *46* (21), 6570–6599.

(45) Blaskovich, M. A. T.; Hansford, K. A.; Gong, Y.; Butler, M. S.; Muldoon, C.; Huang, J. X.; Ramu, S.; Silva, A. B.; Cheng, M.; Kavanagh, A. M.; Ziora, Z.; Premraj, R.; Lindahl, F.; Bradford, T. A.; Lee, J. C.; Karoli, T.; Pelingon, R.; Edwards, D. J.; Amado, M.; Elliott, A. G.; Phetsang, W.; Daud, N. H.; Deecke, J. E.; Sidjabat, H. E.; Ramaooga, S.; Zuegg, J.; Betley, J. R.; Beevers, A. P. G.; Smith, R. A. G.; Roberts, J. A.; Paterson, D. L.; Cooper, M. A. Protein-inspired antibiotics active against vancomycin- and daptomycin-resistant bacteria. *Nat. Commun.* **2018**, *9*, 1 DOI: 10.1038/s41467-017-02123-w.

(46) Antonoplis, A.; Zang, X.; Huttner, M. A.; Chong, K. K. L.; Lee, Y. B.; Co, J. Y.; Amieva, M. R.; Kline, K. A.; Wender, P. A.; Cegelski, L. A Dual-Function Antibiotic-Transporter Conjugate Exhibits Superior Activity in Sterilizing MRSA Biofilms and Killing Persister Cells. *J. Am. Chem. Soc.* **2018**, *140* (47), 16140–16151.

(47) Watanakunakorn, C. The Antibacterial Action of Vancomycin. *Clin. Infect. Dis.* **1981**, *3*, S210–S215.

(48) Allen, N. E.; Hobbes, J. N.; Nicas, T. I. Inhibition of peptidoglycan biosynthesis in vancomycin-susceptible and -resistant bacteria by a semisynthetic glycopeptide antibiotic. *Antimicrob. Agents Chemother.* **1996**, *40* (10), 2356–2362.

(49) Hayami, M.; Okabe, A.; Kariyama, R.; Abe, M.; Kanemasa, Y. Lipid-Composition of *Staphylococcus aureus* and Its Derived L-Forms. *Microbiol. Immunol.* **1979**, *23* (6), 435–442.

(50) Hu, K.; Jiang, Y.; Xie, Y.; Liu, H.; Liu, R.; Zhao, Z.; Lai, R.; Yang, L. Small-Anion Selective Transmembrane "Holes" Induced by an Antimicrobial Peptide Too Short to Span Membranes. *J. Phys. Chem. B* **2015**, *119* (27), 8553–8560.

(51) van Meer, G.; Voelker, D. R.; Feigenson, G. W. Membrane lipids: where they are and how they behave. *Nat. Rev. Mol. Cell Biol.* **2008**, *9* (2), 112–124.

(52) Oren, Z.; Shai, Y. Selective lysis of bacteria but not mammalian cells by diastereomers of melittin: Structure-function study. *Biochemistry* **1997**, *36* (7), 1826–1835.

(53) Som, A.; Yang, L.; Wong, G. C. L.; Tew, G. N. Divalent Metal Ion Triggered Activity of a Synthetic Antimicrobial in Cardiolipin Membranes. *J. Am. Chem. Soc.* **2009**, *131* (42), 15102–151023.

(54) Jiang, Y.; Zheng, W.; Kuang, L.; Ma, H.; Liang, H. Hydrophilic Phage-Mimicking Membrane Active Antimicrobials Reveal Nanostructure-Dependent Activity and Selectivity. *ACS Infect. Dis.* **2017**, *3* (9), 676–687.

(55) Defraigne, V.; Fauvart, M.; Michiels, J. Fighting bacterial persistence: Current and emerging anti-persister strategies and therapeutics. *Drug Resist. Updates* **2018**, *38*, 12–26.

(56) Briers, Y.; Walmagh, M.; Grymonprez, B.; Biebl, M.; Pirnay, J. P.; Defraigne, V.; Michiels, J.; Cenens, W.; Aertsen, A.; Miller, S.; Lavigne, R. Art-175 Is a Highly Efficient Antibacterial against Multidrug-Resistant Strains and Persisters of *Pseudomonas aeruginosa*. *Antimicrob. Agents Chemother.* **2014**, *58* (7), 3774–3784.

(57) Abushahba, M. F. N.; Mohammad, H.; Seleem, M. N. Targeting Multidrug-resistant *Staphylococci* with an anti-rpoA

Peptide Nucleic Acid Conjugated to the HIV-1 TAT Cell Penetrating Peptide. *Mol. Ther. Nucl. Acids* **2016**, *5*, 1 DOI: 10.1038/mtna.2016.53.

(58) Bryskier, A. Anti-MRSA agents: under investigation, in the exploratory phase and clinically available. *Expert Rev. Anti-Infect. Ther.* **2005**, *3* (4), 505–553.